PERGAMON

International Journal of Solids and Structures 36 (1999) 2397–2416

INTERNATIONAL JOURNAL OF SOLIDS and STRUCTURES

A displacement-based reference frame formulation for steady-state thermo-elasto-plastic material processes

D. Balagangadhar[a], G. A. Dorai[a], D. A. Tortorelli[a,b,*]

[a] *Department of Mechanical and Industrial Engineering, University of Illinois at Urbana-Champaign, Urbana IL 61801, U.S.A.*

[b] *Department of Theoretical and Applied Mechanics, University of Illinois at Urbana-Champaign, Urbana IL 61801, U.S.A.*

Received 7 April 1997; in revised form 30 January 1998

Abstract

A reference frame formulation for steady state thermo-elasto-plastic processes is presented. The displacement and history dependent response fields appear as the primary variables in this mixed formulation. Unlike displacement based Lagrangian formulations, our formulation does not require a transient analysis to simulate a steady state process and yields results that are free of numerical oscillations and which require considerably less computational effort. And unlike velocity based Eulerian methods, our formulation does not require free surface corrections or streamline integration algorithms. A laser surface treatment process is simulated and our results are in agreement with those obtained from a computationally intensive transient Lagrangian analysis.

1. Introduction

Many manufacturing processes such as laser surface treatment, metal forming, continuous casting, etc., are steady state in nature. Materials used in these processes exhibit history dependent response e.g. plasticity. Hence, the analyst must consider the deformation history which each material particle experiences, even though the process is steady state. This material history is not an issue in fluids problems e.g. the flow of a Newtonian fluid through a pipe.

Traditionally steady state processes, with history dependent material behavior, have been analyzed using Lagrangian kinematic descriptions (Lee et al., 1976; Appleby et al., 1984; Carroll and Strenkowski, 1988), in which the displacement is the primary variable. This method requires a transient analysis to determine the evolution of the history dependent variables. The transient analysis terminates when 'steady-state' behavior is observed. However, oscillations appear in the computed 'steady-state' Lagrangian fields due to the interaction between the time and space

* Corresponding author. Fax: 001 217 244 6534; e-mail: dtort@acm6.me.uiuc.edu

0020–7683/99/ - see front matter
PII: S0020–7683(98)00065–1

discretizations (Appleby et al., 1984). Moreover, these methods are computationally inefficient since they require meshes and transient analysis.

Local mesh refinement is often required to accurately compute the solution and to eliminate the inefficiencies due to uniform mesh refinement (IJNME, 1991; CMAME, 1992). The regions that require refinement are often known a priori. Consequently in the steady analysis, the appropriate refinement can be implemented. However in transient analyses considered here, the refined regions evolve and therefore adaptive meshing schemes are required (IJNME, 1991; CMAME, 1992; Palle, 1993). This requirement further taxes the computational effort associated with Lagrangian steady state analyses.

Steady state processes have also been modeled using Eulerian kinematic descriptions (Zienkiewicz and Godbole, 1974; Zienkiewicz et al., 1978; Strenkowski and Moon, 1990; Ruan, 1996). Most of these formulations, which use velocity as the primary field, assume viscoplastic material behavior and neglect elastic deformation (Zienkiewicz and Godbole, 1974; Zienkiewicz et al., 1978). If necessary, elastic strain effects can be included by an 'elastic reanalysis' (Zienkiewicz et al., 1978) or by the 'initial stress-rate method' (Dawson and Thompson, 1978).

In Eulerian formulations for steady state processes, the history dependent variables can be evaluated by integrating the evolution equations along their path-lines (Viriyauthakorn and Caswell, 1980; Dawson, 1978). This integration requires that the path-lines be known a priori and hence, iterations are performed in which the momentum balance equations are solved to determine the path-lines and the evolution equations are integrated to determine the material response. In contrast to this iterative technique which requires two distinct analyses, the material response evolution equations can be solved simultaneously with the momentum balance equation via the Galerkin method (Thompson et al., 1983). The strengths and limitations of these two models are discussed by Agrawal and Dawson (Agrawal and Dawson, 1985). They note that, while both methods yield accurate results, the numerical implementation of the latter method is simpler than that of the path-line integration method. However, results obtained from the latter method exhibit oscillations (Agrawal and Dawson, 1985) due to the hyperbolic nature of the evolution equations. Recently, these oscillations have been resolved using the streamline upwind Petrov–Galerkin method (Ruan, 1996).

Another issue in velocity based Eulerian formulations is the treatment of free surfaces. Since the governing equations are expressed on the deformed configuration, the surfaces on the control volume that are loaded with tractions must be adjusted to coincide with the surface path-lines. This adjustment is accomplished by either iterative updating or successive recalculation (Dawson and Thompson, 1978); both are time consuming tasks.

Arbitrary Lagrangian–Eulerian (ALE) kinematic descriptions, which combine both the Eulerian and Lagrangian descriptions, have also been used to solve history-dependent problems (Heutink et al., 1990; Rakotomalala and Joyot, 1993; Hu and Liu, 1993; Liu et al. 1986; Liu et al. 1988; Haber, 1984; Lee and Haber, 1993; Ghosh and Kikuchi, 1991; Ghosh and Suresh, 1996). In such descriptions, the finite elements need not adhere to a fixed material volume nor to a fixed control volume. ALE formulations are suitable for problems where the region of interest moves in a fixed domain, such as in crack propagation (Lee and Haber, 1993). The formulation requires a transient analysis for history-dependent problems. Both velocity based (Rakotomalala and Joyot, 1993; Hu and Liu, 1993; Liu et al., 1986; Liu et al., 1988) and displacement based (Haber 1984; Lee and Haber, 1993; Ghosh and Kikuchi, 1991; Ghosh and Suresh, 1996) ALE formulations have been reported.

In this work, we use a Reference Frame kinematic description to take advantage of the steady-state nature of some manufacturing processes. We use displacement as the primary field, instead of velocity, thereby obviating the need for free surface corrections and streamline integrations. History dependent response fields (the plastic strain and cumulative plastic strain) also appear as primary variables, in what is now a mixed formulation. The hyperbolic material evolution equations are solved via the streamline upwind Petrov–Galerkin method (Brooks and Hughes, 1982; Ruan, 1996) to eliminate the oscillations that are reported in prior numerical studies. The solution of the steady state problem via the Eulerian formulation requires the appropriate specification of boundary conditions over the control volume's inlet and outlet surfaces. We prescribe traction and surface flux boundary conditions at these surfaces to be consistent with the steady-state response fields.

To exemplify the analysis, we simulate a laser surface treatment process. A simplified two-dimensional plane strain model is used to represent the geometry and the J_2 flow theory is used to model the material response. Small deformations are assumed in this steady state analysis in which the laser passes over the work piece at a constant velocity thereby inducing the thermal load which causes the deformation. The results of our steady-state analysis are in agreement with those obtained from a transient ABAQUS (ABAQUS 5.6, 1996) analysis. The advantages of the Reference Frame method vs the Lagrangian method are apparent as the computational effort is reduced by an order of magnitude.

2. Reference frame kinematic model

The body is in configuration V at time $t = 0$ and its material particles are identified in V via the position vector $\mathbf{X}$, defined with respect to the material coordinate frame $\{\mathbf{0} : \mathbf{e}_1, \mathbf{e}_2, \mathbf{e}_3\}$. Here, $\{\mathbf{e}_1, \mathbf{e}_2, \mathbf{e}_3\}$ comprises an orthonormal basis. The motion of the body is represented by the smooth mapping $\mathbf{f}$ such that at any given time $t \in I$, the location $\mathbf{x}$ (with respect to the material coordinate frame) of a material point which occupied the position $\mathbf{X}$ at time $t = 0$ in V is given by

$$\mathbf{x} = \mathbf{f}(\mathbf{X}, t) \tag{1}$$

Here $I = [0, T]$ is the time interval in which the problem is defined and T is the terminal time in the analysis. The mappings $\mathbf{f}$ and the position vector $\mathbf{X}$ and $\mathbf{x}$ are illustrated in Fig. 1. We emphasize that the material frames used to define $\mathbf{X}$ and $\mathbf{x}$ are one and the same.

In most steady state processes, the region over which the deformation evolves is primarily restricted to the vicinity of the loading. We represent this region by V_0 in the undeformed configuration; V_0 corresponds to the configuration V_t in the deformed configuration (see Fig. 1), i.e. $V_t = \mathbf{f}(V_0, t)$. One may think of V_0 as a control volume, however here it is not associated with the deformed configuration (as in a Eulerian analysis), rather it is associated with the undeformed configuration (as in a Lagrangian analysis).

We now introduce a reference configuration V_r. Material particles are identified in V_r via the position vector $\mathbf{r}$, defined with respect to its distinct reference coordinate frame $\{\hat{\mathbf{0}} : \hat{\mathbf{e}}_1, \hat{\mathbf{e}}_2, \hat{\mathbf{e}}_3\}$, where $\{\hat{\mathbf{e}}_1, \hat{\mathbf{e}}_2, \hat{\mathbf{e}}_3\}$ comprises an orthonormal basis. At any given time t, V_r is mapped into the undeformed configuration V_0 by the map $\mathbf{g}$ (see Fig. 1). Note that V_r only maps to the control volume

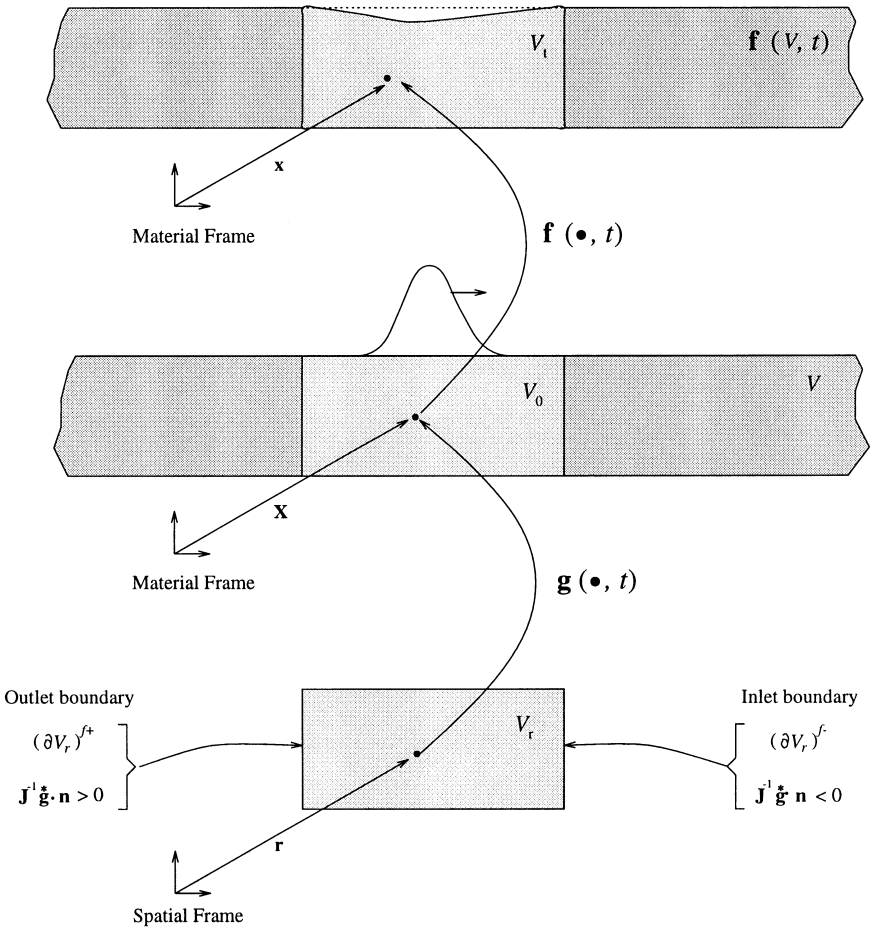

Fig. 1. Kinematic model.

portion of the undeformed body and this portion changes in time to follow the loading zone i.e., $V_0 = \mathbf{g}(V_r, t)$. The position vectors $\mathbf{r}$ in the reference configuration and $\mathbf{X}$ in the undeformed configuration are related by

$$\mathbf{X} = \mathbf{g}(\mathbf{r}, t) \tag{2}$$

The Jacobian associated with this mapping is defined as

$$\mathbf{J}(\mathbf{r}, t) = \frac{\partial \mathbf{g}}{\partial \mathbf{r}}(\mathbf{r}, t) \tag{3}$$

and the determinant of the Jacobian is denoted by J, i.e. $J(\mathbf{r}, t) = \det(\mathbf{J}(\mathbf{r}, t))$.

On the reference configuration, we define the inlet boundary $(\partial V_r)^{f-}$ as the subsurface of ∂V_r over which material flows into the domain i.e. $\overset{*}{\mathbf{g}}\cdot\mathbf{n} < 0$ [or $\mathbf{J}^{-1}\overset{*}{\mathbf{g}}\cdot\mathbf{n}_r < 0$ by Nanson's formula (Ogden, 1984)]. The outflow boundary $(\partial V_r)^{f+} \subset \partial V_r$ is similarly defined as the subsurface over

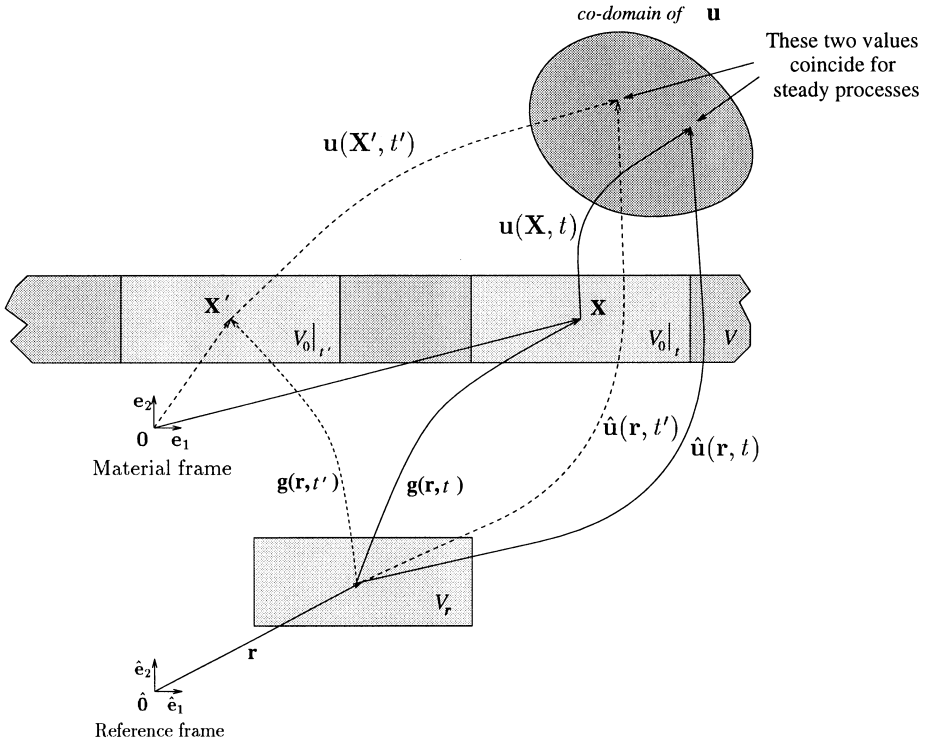

Fig. 2. Definition of composite functions.

which the material exits the domain i.e. $\overset{*}{\mathbf{g}}\cdot\mathbf{n} > 0$ (or $\mathbf{J}^{-1}\overset{*}{\mathbf{g}}\cdot\mathbf{n}_r > 0$). Here $\mathbf{n}$ and $\mathbf{n}_r$ are the normals to the surface ∂V and ∂V_r, respectively.

Fields defined on the undeformed configuration V_0 (i.e. material fields) are denoted as $(\,)(\mathbf{X}, t)$, and for each of these fields we define the corresponding reference field $\hat{(\,)}(\mathbf{r}, t)$ on V_r such that their values are equal at corresponding points (see Fig. 2), i.e.

$$\hat{(\,)}(\mathbf{r}, t) = (\,)(\mathbf{g}(\mathbf{r}, t), t) \tag{4}$$

Note that at different times, e.g. t and t', the material point associated with $\mathbf{r}$ changes, e.g. $\mathbf{X} = \mathbf{g}(\mathbf{r}, t)$ and $\mathbf{X}' = \mathbf{g}(\mathbf{r}, t')$, and hence the reference fields when evaluated at $(\mathbf{r}, t)$ and $(\mathbf{r}, t')$ will generally not be equal. If the function values for the pairs $(\mathbf{r}, t)$ and $(\mathbf{r}, t')$ agree for all $\mathbf{r}$ in V_r and for all t in I, then the process is deemed steady and we have e.g. $\hat{\mathbf{u}}(\mathbf{r}, t) = \hat{\mathbf{u}}(\mathbf{r}, t')$; and consequently $\mathbf{u}(\mathbf{X}, t) = \mathbf{u}(\mathbf{X}', t')$.

We adopt the following notation for gradient operators for fields defined over the undeformed and reference configurations.

$$\nabla_{\mathbf{x}}(\,)(\mathbf{X}, t) = \frac{\partial(\,)}{\partial \mathbf{X}}(\mathbf{X}, t)\,; \quad \nabla_{\mathbf{r}}\hat{(\,)}(\mathbf{r}, t) = \frac{\partial \hat{(\,)}}{\partial \mathbf{r}}(\mathbf{r}, t) \tag{5}$$

Similarly, we define partial derivatives with respect to time for fields defined over the undeformed and reference configurations

$$\frac{\partial(\,)}{\partial t}(\mathbf{X},t)=\dot{(\,)}(\mathbf{X},t)\,;\quad \frac{\partial\hat{(\,)}}{\partial t}(\mathbf{r},t)=\overset{*}{\hat{(\,)}}(\mathbf{r},t) \tag{6}$$

Note that $\dot{(\,)}(\mathbf{X},t)$ is the usual material time derivative.

3. Lagrangian formulation for thermo-elasto-plasticity

In this section, we present the initial boundary value problem (IBVP) associated with thermo-elasto-plastic quasi-static bodies. We restrict our discussion to those problems in which the temperature solution can be solved prior to the mechanical problem i.e., weak coupling is assumed. We also neglect inertial effects in the momentum balance equation. Finally, we assume that the displacement gradients are small and use the linearized governing equations. As such, all equations and fields are defined on the undeformed material configuration V. The conventional IBVP for thermal and mechanical analyses are presented in Sections 3.1 and 3.2, respectively.

3.1. Thermal analysis

The body with initial temperature field θ^0, density ρ, internal energy e, and conductivity tensor $\mathbf{K}$, is subjected to a heat source r within V and to prescribed temperature $\bar{\theta}$ and surface flux $\bar{q}$ boundary conditions on the complementary subsurfaces ∂V^θ and ∂V^q of ∂V, respectively. To solve the thermal IBVP for the temperature θ, we must satisfy the following governing equations, boundary conditions and initial conditions

$$\begin{aligned}
-\mathrm{div}_{\mathbf{x}}\, q(\mathbf{X},t)+r(\mathbf{X},t) &= \rho\frac{\mathrm{d}e}{\mathrm{d}t}(\mathbf{X},t) && \text{in } V\times I\\
\mathbf{q}(\mathbf{X},t) &= -\mathbf{K}(\mathbf{X},t)\frac{\partial\theta}{\partial\mathbf{X}}(\mathbf{X},t) && \text{on } V\times I\\
\mathbf{q}(\mathbf{X},t)\cdot\mathbf{n}(\mathbf{X},t) &= \bar{q}(\mathbf{X},t) && \text{on } \partial V^q\times I\\
\theta(\mathbf{X},t) &= \bar{\theta}(\mathbf{X},t) && \text{on } \partial V^\theta\times I\\
\theta(\mathbf{X},t) &= \theta^0(\mathbf{X}) && \text{on } V
\end{aligned} \tag{7}$$

where $\mathbf{q}$ denotes the heat flux vector, $\mathrm{div}_{\mathbf{x}}$ denotes the divergence with respect to the position $\mathbf{x}$, and $\mathrm{d}/\mathrm{d}t$ denotes the material time derivative.

3.2. Mechanical analysis

The strain $\mathbf{E}$ is obtained from the displacement field $\mathbf{u}$ using the infinitesimal strain–displacement relation.

$$\mathbf{E}(\mathbf{X},t)=\frac{1}{2}\left[\frac{\partial\mathbf{u}}{\partial\mathbf{X}}(\mathbf{X},t)+\left(\frac{\partial\mathbf{u}}{\partial\mathbf{X}}(\mathbf{X},t)\right)^T\right]\quad\text{in } V\times I \tag{8}$$

Additionally, $\mathbf{E}$ is assumed to be the sum of elastic, plastic and thermal strains denoted as $\mathbf{E}_e$, $\mathbf{E}_p$ and $\mathbf{E}_\theta$, respectively, so that we also have

$$\mathbf{E}(\mathbf{X},t) = \mathbf{E}_e(\mathbf{X},t) + \mathbf{E}_p(\mathbf{X},t) + \mathbf{E}_\theta(\mathbf{X},t) \quad \text{in } V\times I \tag{9}$$

The thermal strain $\mathbf{E}_\theta$ results from thermal expansion, i.e.

$$\mathbf{E}_\theta(\mathbf{X},t) = (\theta(\mathbf{X},t)-\theta_r)\mathbf{M}(\mathbf{X}) \quad \text{in } V\times I \tag{10}$$

where θ_r is a uniform reference temperature and $\mathbf{M}$ is a constant and diagonal tensor field which dictates the thermal expansion. The plastic strain $\mathbf{E}_p$ results from the permanent plastic deformation due to the movement of dislocations along crystallographic planes (Lubliner, 1990).

Following the usual assumptions that neither the thermal nor the plastic strains contribute to the Cauchy stress $\mathbf{S}$ (Lubliner, 1990), we have

$$\mathbf{S}(\mathbf{X},t) = \mathbf{C}(\mathbf{X})[\mathbf{E}_e(\mathbf{X},t)] = \mathbf{C}(\mathbf{X})[\mathbf{E}(\mathbf{X},t)-\mathbf{E}_p(\mathbf{X},t)-\mathbf{E}_\theta(\mathbf{X},t)] \quad \text{in } V\times I \tag{11}$$

where $\mathbf{C}$ is the constant elasticity tensor.

For simplicity, we incorporate the associative J_2 plasticity theory (Lubliner, 1990). Accordingly, the von Mises pressure insensitive yield criterion f, the evolutions of the plastic strain $\mathbf{E}_p$ and the cumulative plastic strain ε are given by

$$\begin{aligned} f(\mathbf{S}_d,\varepsilon) &= \|\mathbf{S}_d\| - \sqrt{\tfrac{2}{3}}\kappa(\varepsilon) \leqslant 0 && \text{on } V\times I \\ \dot{\mathbf{E}}_p(\mathbf{X},t) &= \alpha(\mathbf{X},t)[\mathbf{N}(\mathbf{X},t)\otimes\mathbf{N}(\mathbf{X},t)]\dot{\mathbf{E}}(\mathbf{X},t) && \text{in } V\times I \\ \dot{\varepsilon}(\mathbf{X},t) &= \sqrt{\tfrac{2}{3}}\,\|\dot{\mathbf{E}}_p(\mathbf{X},t)\| && \text{in } V\times I \end{aligned} \tag{12}$$

where $\mathbf{S}_d = \mathbf{S} - \frac{1}{3}(\mathbf{S}\cdot\mathbf{I})\mathbf{I}$ is the deviatoric stress tensor, κ is the hardening rule obtained from a uniaxial tension test, $\mathbf{N} = \mathbf{S}_d/\|\mathbf{S}_d\|$ is the normalized gradient of the yield function with respect to $\mathbf{S}_d$,

$$\alpha = \begin{cases} 0 & \text{if } f \leqslant 0 \text{ or } \dot{f} \leqslant 0 \\ \dfrac{1}{1+\dfrac{\kappa'}{3G}} & \text{otherwise} \end{cases} \tag{13}$$

and G is the shear modulus.

The body is subjected to a body force $\mathbf{b}$ and thermal loads within V and to displacement $\bar{\mathbf{u}}$ and traction $\bar{\mathbf{t}}$ boundary conditions prescribed on the complementary subsurfaces ∂V^u and ∂V^t of ∂V, respectively. To solve the IBVP, we must satisfy the previous equations along with the following equilibrium equation, boundary conditions and initial conditions (on the plastic strain $\mathbf{E}_p^0$, and cumulative plastic strain ε^0)

$$\begin{aligned} \operatorname{div}_{\mathbf{x}}\mathbf{S}(\mathbf{X},t) + \mathbf{b}(\mathbf{X},t) &= \mathbf{0} && \text{in } V\times I \\ \mathbf{u}(\mathbf{X},t) &= \bar{\mathbf{u}}(\mathbf{X},t) && \text{on } \partial V^u\times I \\ \mathbf{S}(\mathbf{X},t)\mathbf{n}(\mathbf{X},t) &= \bar{\mathbf{t}}(\mathbf{X},t) && \text{on } \partial V^t\times I \end{aligned}$$

$$\mathbf{E}_p(\mathbf{X},0) = \mathbf{E}_p^0(\mathbf{X}) \quad \text{on } V$$
$$\varepsilon(\mathbf{X},0) = \varepsilon^0(\mathbf{X}) \quad \text{on } V \tag{14}$$

These equations hold for any subdomain of V, in particular the subregion V_t, encompassing the loading zone as illustrated in Fig. 1. We note that the evolution of the state variables, $\mathbf{E}_p$ and ε, is dependent on the loading path, i.e. they are history dependent.

We emphasize that we use displacements as the primary variable and that the IBVP is defined over the known undeformed configuration. This formulation contrasts velocity based formulations that define the IBVP over the deformed configuration, which is not known a priori for the type of problems we consider.

4. Reference Frame formulation for steady state processes

The kinematic description and the transformation equations of Section 2 are used to express the IBVP on the Reference Frame. We then specialize the previous derivation for steady state processes. In Section 4.1, we express the governing equations developed in Section 3 using the Reference Frame kinematic description. The theory is specialized for steady state processes in Section 4.2.

4.1. Transformation to reference configuration

The governing equations of Section 3 are now transformed to the reference configuration. The analysis is subsequently performed on the reference configuration to evaluate the reference fields. Equation (4) is then used to evaluate the corresponding field quantities on the undeformed configuration.

The thermal IBVP transforms as

$$\begin{aligned}
-\mathrm{div}_{\mathbf{r}}\,[J\mathbf{J}^{-1}\hat{\mathbf{q}}] + J\hat{r} &= J\rho[\overset{*}{\hat{e}} - \nabla_{\mathbf{r}}\hat{e}\cdot\mathbf{J}^{-1}\overset{*}{\mathbf{g}}] && \text{in } V_r\times I\\
\hat{\mathbf{q}} &= -\hat{\mathbf{K}}\mathbf{J}^{-T}\nabla_{\mathbf{r}}\hat{\theta} && \text{in } V_r\times I\\
\hat{\theta} &= \bar{\theta}|_{\mathbf{x}=\mathbf{g}(\mathbf{r},t)} && \text{on } \partial V_r^{\theta}\times I\\
J\mathbf{J}^{-1}\hat{\mathbf{q}}\cdot\mathbf{n}_r &= J\|\mathbf{J}^{-T}\mathbf{n}\|\,\bar{q}|_{\mathbf{x}=\mathbf{g}(\mathbf{r},t)} && \text{on } \partial V_r^{q}\times I\\
\hat{\theta} &= \theta^0|_{\mathbf{x}=\mathbf{g}(\mathbf{r},0)} && \text{on } V_r
\end{aligned} \tag{15}$$

where $\mathrm{div}_{\mathbf{r}}$ denotes the divergence with respect to the reference position $\mathbf{r}$; $\partial V^{\theta} = \mathbf{g}(\partial V_r^{\theta}, t)$ and similarly $\partial V^{q} = \mathbf{g}(\partial V_r^{q}, t)$. Note that some of the boundary conditions correspond to the inlet and outlet surfaces of the loaded body (see Fig. 1); hence their values are not easily prescribed. We discuss this matter further in Section 4.2 where we specialize the theory to steady state processes.

We now use eqns (4)–(6) to transform the mechanical IBVP to the reference configuration. Equations (8)–(12) transform as

$$\left.\begin{aligned}
\hat{\mathbf{E}} &= \hat{\mathbf{E}}_e + \hat{\mathbf{E}}_p + \hat{\mathbf{E}}_\theta \\
\hat{\mathbf{E}}_\theta &= [\hat{\theta} - \theta_0]\hat{\mathbf{M}} \\
\hat{\mathbf{S}} = \hat{\mathbf{C}}[\hat{\mathbf{E}}_e] &= \hat{\mathbf{C}}[\hat{\mathbf{E}} - \hat{\mathbf{E}}_p - \hat{\mathbf{E}}_\theta] \\
f(\hat{\mathbf{S}}_d, \hat{\varepsilon}) &= \|\hat{\mathbf{S}}_d\| - \sqrt{\tfrac{2}{3}}\kappa(\hat{\varepsilon}) \leqslant 0 \\
\hat{\mathbf{E}} &= \tfrac{1}{2}(\nabla_{\mathbf{r}}\mathbf{u}\mathbf{J}^{-1} + (\nabla_{\mathbf{r}}\mathbf{u}\mathbf{J}^{-1})^T) \\
\overset{*}{\hat{\mathbf{E}}}_p - \nabla_{\mathbf{r}}\hat{\mathbf{E}}_p\mathbf{J}^{-1}\overset{*}{\mathbf{g}} &= \alpha(\mathbf{N}\otimes\mathbf{N})[\overset{*}{\hat{\mathbf{E}}} - \nabla_{\mathbf{r}}\hat{\mathbf{E}}\mathbf{J}^{-1}\overset{*}{\mathbf{g}}] \\
\overset{*}{\hat{\varepsilon}} - \nabla_{\mathbf{r}}\hat{\varepsilon}\mathbf{J}^{-1}\overset{*}{\mathbf{g}} &= \sqrt{\tfrac{2}{3}}\|\overset{*}{\hat{\mathbf{E}}}_p - \nabla_{\mathbf{r}}\hat{\mathbf{E}}_p\mathbf{J}^{-1}\overset{*}{\mathbf{g}}\|
\end{aligned}\right\} \quad \text{on } V_r \times I \tag{16}$$

and G is replaced and $\hat{G}$ in eqn (13). The equilibrium equation and boundary conditions transform as

$$\begin{aligned}
\operatorname{div}_{\mathbf{r}}[J\hat{\mathbf{S}}\mathbf{J}^{-1}] + J\hat{\mathbf{b}} &= \mathbf{0} && \text{in } V_r \times I \\
\hat{\mathbf{u}} &= \bar{\mathbf{u}}|_{\mathbf{X}=\mathbf{g}(\mathbf{r},t)} && \text{on } \partial V_r^u \times I \\
J\hat{\mathbf{S}}(\mathbf{r},t)\mathbf{J}^{-T}\mathbf{n}_r &= J\|\mathbf{J}^{-T}\mathbf{n}_r\|\bar{\mathbf{t}}|_{\mathbf{X}=\mathbf{g}(\mathbf{r},t)} && \text{on } \partial V_r^t \times I
\end{aligned} \tag{17}$$

where $\partial V^u = \mathbf{g}(\partial V_r^u, t)$ and similarly $\partial V^t = \mathbf{g}(\partial V_r^t, t)$. Note that, like the thermal boundary conditions, the mechanical boundary conditions may be difficult to prescribe over the inlet and outlet surfaces of the loaded body. We again defer the discussion of this matter until Section 4.2.

The initial conditions of the reference configuration, are obtained from the initial conditions on the image of $\mathbf{g}(V_r, 0)$, i.e.,[1]

$$\begin{aligned}
\hat{\mathbf{E}}_p(\mathbf{r},0) &= \mathbf{E}_p^0(\mathbf{g}(\mathbf{r},0)) \quad \text{on } V_r \\
\hat{\varepsilon}(\mathbf{r},0) &= \varepsilon^0(\mathbf{g}(\mathbf{r},0)) \quad \text{on } V_r
\end{aligned} \tag{18}$$

The presence of the convective terms in the evolution equations of ε and $\mathbf{E}_p$ [cf eqns $(16)_6$ and $(16)_7$], yields a hyperbolic problem. Hence, we must also specify the current values of the history dependent state variables ($\hat{\mathbf{E}}_p$ and $\hat{\varepsilon}$) for all material particles that enter the domain across the inlet boundary $(\partial V_r)^{f-}$, i.e. we prescribed the following boundary conditions

$$\begin{aligned}
\hat{\mathbf{E}}_p(\mathbf{r},t) &= \bar{\mathbf{E}}_p(\mathbf{r},t) \quad \text{on } (\partial V_r)^{f-} \\
\hat{\varepsilon}(\mathbf{r},t) &= \bar{\varepsilon}(\mathbf{r},t) \quad \text{on } (\partial V_r)^{f-}
\end{aligned} \tag{19}$$

These boundary conditions, like those in eqns $(17)_2$ and $(17)_3$, may be difficult to prescribe.

4.2. Steady state processes

We now specialize the theory developed in the previous section for the two-dimensional steady state process shown in Fig. 3. A semi-infinite domain V with a uniform initial temperature field θ_0, zero initial plastic strain (i.e. $\mathbf{E}_p^0 = 0$ and $\varepsilon^0 = 0$) and zero residual stress is subjected to a moving

[1] As seen in the next section, these initial conditions are not required in the steady state analysis.

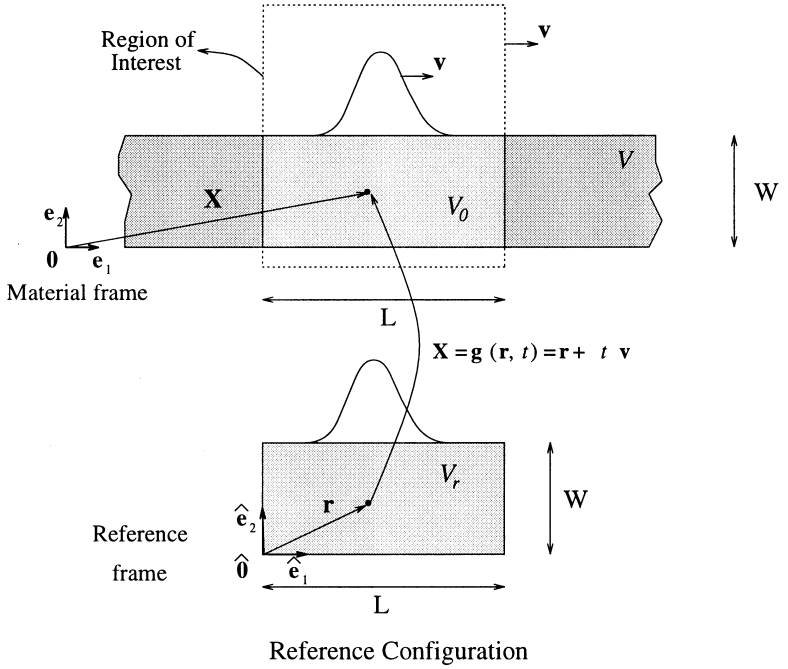

Fig. 3. Kinematic model for the steady state problem.

load with a constant velocity $\mathbf{v}$. The material coordinate system is defined so that the $\mathbf{e}_1$ axis and $\mathbf{v}$ are aligned, i.e., $\mathbf{v} = v\mathbf{e}_1$, where v is the magnitude of the velocity and $\mathbf{e}_1$–$\mathbf{e}_2$ plane is the plane over which the plane strain analysis is performed. The material domain of interest V_0 encompasses and translates with the load region. The length of V_0 is chosen so that the inlet edge is significantly ahead of the loading zone and the outlet edge is significantly away of the loading zone so that the material fields at the outlet edge are sufficiently uniform in the X_1 direction (here $X_i = \mathbf{X}\cdot\mathbf{e}_i$).

The reference configuration, V_r, is of the same length (L) and breadth (W) as V_0 and is oriented such that $\hat{\mathbf{e}}_i$ is mapped into $\mathbf{e}_i$, i.e.

$$\mathbf{X} = \mathbf{g}(\mathbf{r}, t) = \mathbf{r} + t\mathbf{v} \tag{20}$$

Trivially then, $\mathbf{J} = \mathbf{I}$ and $\mathbf{J}^{-1}\overset{*}{\mathbf{g}} = \mathbf{v}$; and the inflow and outflow boundaries are identified as

$$(\partial\mathbf{V}_r)^{f^-} = \{\mathbf{r} : r_1 = L\}; \quad (\partial\mathbf{V}_r)^{f^+} = \{\mathbf{r} : r_1 = 0\} \tag{21}$$

where $r_i = \mathbf{r}\cdot\hat{\mathbf{e}}_i$.

Since the reference configuration translates with the load zone, the reference fields do not vary with time, i.e. $\overset{*}{(\ )}(\mathbf{r}, t) = 0$ and hence the reference IBVP becomes a steady-state boundary value problem (BVP). The thermal IBVP now reduces to

$$\begin{aligned} -\mathrm{div}_{\mathbf{r}}\,\hat{\mathbf{q}} + \hat{r} &= -\frac{\partial\hat{e}}{\partial r_1}v \quad \text{in } V_r \\ \hat{\mathbf{q}} &= -\hat{\mathbf{K}}\nabla_{\mathbf{r}}\hat{\theta} \quad \text{in } V_r \end{aligned} \tag{22}$$

where $[\partial(\hat{\ })/\partial r_i] = \nabla_{\mathbf{r}}(\hat{\ }) \cdot \hat{\mathbf{e}}_i$ and the temperature field, $\hat{\theta}$ is now defined on V_r and no longer on $V_{r\times I}$. Flux boundary conditions are prescribed on the inlet and outlet surfaces i.e. $(\partial V_r)^{f^-}$ and $(\partial V_r)^{f^+}$. Since the temperature field is assumed to be sufficiently uniform in the $\hat{\mathbf{e}}_1$ direction near the inlet and outlet edges, a zero surface flux is prescribed across these boundaries. On the remainder of the boundary, either flux or temperature boundary conditions are prescribed.

$$\begin{aligned}
\hat{\theta} &= \bar{\theta} \quad \text{on } \partial V_r^{\theta} \\
\hat{\mathbf{q}} \cdot \mathbf{n}_r &= 0 \quad \text{on } ((\partial V_r)^{f^-} + (\partial V_r)^{f^+}) \subset \partial V_r^{q} \\
\hat{\mathbf{q}} \cdot \mathbf{n}_r &= \bar{q} \quad \text{on } \partial V_r^{q} - ((\partial V_r)^{f^-} + (\partial V_r)^{f^+})
\end{aligned} \tag{23}$$

The mechanical IBVP is now expressed as

$$\left.\begin{aligned}
\operatorname{div}_{\mathbf{r}} \hat{\mathbf{S}} + \hat{\mathbf{b}} &= \mathbf{0} \\
\hat{\mathbf{S}} &= \hat{\mathbf{C}}[\hat{\mathbf{E}} - \hat{\mathbf{E}}_p - \hat{\mathbf{E}}_{\theta}] \\
\hat{\mathbf{E}} &= \tfrac{1}{2}(\nabla_r \hat{\mathbf{u}} + (\nabla_r \hat{\mathbf{u}})^T) \\
\frac{\partial \hat{\mathbf{E}}_p}{\partial r_1} &= \alpha(\hat{\mathbf{N}} \otimes \hat{\mathbf{N}}) \frac{\partial \hat{\mathbf{E}}}{\partial r_1} \\
-\frac{\partial \hat{\varepsilon}}{\partial r_1} &= \sqrt{\frac{2}{3}} \left\| \frac{\partial \hat{\mathbf{E}}_p}{\partial r_1} \right\|
\end{aligned}\right\} \quad \text{on } V_r \tag{24}$$

where all fields are solely defined on V_r and no longer on $V_r \times I$. Traction boundary conditions are prescribed at the inlet and outlet surfaces i.e. $(\partial V_r)^{f^-}$ and $(\partial V_r)^{f^+}$, to mimic the stress state at these locations in the undeformed configuration. Since $(\partial V_r)^{f^-}$ is significantly ahead of the loading zone, and since the unloaded body has zero plastic strain and stress, we apply the following boundary conditions at the inlet.

$$\left.\begin{aligned}
\hat{\mathbf{E}}_p &= \mathbf{0} \\
\hat{\varepsilon} &= 0 \\
\hat{\mathbf{S}}\hat{\mathbf{n}}_r &= \mathbf{0}
\end{aligned}\right\} \quad \text{on } (\partial V_r)^{f^-} \tag{25}$$

Over the outlet $(\partial V_r)^{f^+}$, we use the facts that the fields are sufficiently developed, and that the flux fields are uniform in the $\hat{\mathbf{e}}_1$-direction. In particular, the stress field is uniform in the $\hat{\mathbf{e}}_1$-direction, hence we are able to prescribe the value of $\bar{\mathbf{t}}$ (see Section 5 for details) across $(\partial V_r)^{f^+}$

$$\hat{\mathbf{S}}(\mathbf{r})\mathbf{n}_r(\mathbf{r}) = \bar{\mathbf{t}}(\mathbf{g}(\mathbf{r}, t), t) \quad \text{on}(\partial V_r)^{f^+} \tag{26}$$

Over the remainder of the boundary, we prescribe either traction or displacement

$$\begin{aligned}
\hat{\mathbf{u}}(\mathbf{r}) &= \bar{\mathbf{u}}(\mathbf{g}(\mathbf{r}, t), t) \quad \text{on } \partial V_r^{u} \\
\hat{\mathbf{S}}(\mathbf{r})\mathbf{n}_r(\mathbf{r}) &= \bar{\mathbf{t}}(\mathbf{g}(\mathbf{r}, t), t) \quad \text{on } \partial V_r^{t} - ((\partial V_r)^{f^+} + (\partial V_r)^{f^-})
\end{aligned} \tag{27}$$

After this reference BVP is solved, the material fields are computed through eqn (4), e.g. $\mathbf{E}_p(\mathbf{g}(\mathbf{r}, t), t) = \hat{\mathbf{E}}_p(\mathbf{r})$ at any time t (cf Fig. 2). In our kinematic description for steady state processes,

the reference and undeformed configurations coincide. Therefore, one can view the response of the reference configuration to be that of the undeformed configuration associated with it at a given instant.

5. Weak formulation

The method of weighted residuals is used to develop a weak formulation for the thermomechanical BVP. The heat flux eqn $(22)_2$ and temperature boundary conditions $(23)_1$ are strongly enforced, while the energy balance eqn $(22)_1$ and the heat flux boundary conditions $(23)_{2-3}$ are weakly enforced through the residual

$$R_\theta(\hat{\theta},\tilde{\theta}) = \int_{V_r} \nabla_{\mathbf{r}}\tilde{\theta}\cdot\hat{\mathbf{K}}\nabla_{\mathbf{r}}\hat{\theta}\,\mathrm{d}V_r - \int_{V_r}\tilde{\theta}\frac{\partial\hat{e}}{\partial r_1}v\,\mathrm{d}V_r - \int_{V_r}\tilde{\theta}\hat{r}\,\mathrm{d}V_r - \int_{\partial V_r^q}\tilde{\theta}\bar{q}\,\mathrm{d}A_r \tag{28}$$

where $\tilde{\theta}$ is a suitable arbitrary weighting function. We note that, though the thermal governing eqn $(22)_1$ is a mixed elliptic–hyperbolic equation, the exact solution to the thermal BVP is smooth and hence the standard Galerkin method produces acceptable results (Johnson, 1987).

In the weak formulation for the mechanical problem, eqns $(24)_2$ and $(24)_3$, and the displacement boundary conditions are strongly enforced, whereas eqns $(24)_1$, $(24)_4$ and $(24)_5$, and the traction boundary conditions are weakly enforced. The result is mixed formulation, in which $\hat{\boldsymbol{\Xi}} = (\hat{\mathbf{u}}, \hat{\mathbf{E}}_p, \hat{\varepsilon})$ is the independent variable, implicitly defined by the following three residuals

$$R_{\mathbf{u}}(\hat{\boldsymbol{\Xi}},\tilde{\boldsymbol{\Xi}}) = \int_{V_r}\tilde{\mathbf{E}}\cdot(\hat{\mathbf{C}}[\hat{\mathbf{E}}-\hat{\mathbf{E}}_p-\hat{\mathbf{E}}_t])\,\mathrm{d}V_r - \int_{V_r}\tilde{\mathbf{u}}\cdot\hat{\mathbf{b}}\,\mathrm{d}V_r - \int_{\partial V_r^t}\tilde{\mathbf{u}}\cdot\bar{\mathbf{t}}\,\mathrm{d}A_r \tag{29}$$

$$R_{\mathbf{E}_p}(\hat{\boldsymbol{\Xi}},\tilde{\boldsymbol{\Xi}}) = \int_{V_r}\left(\tilde{\mathbf{E}}_p+\beta v\frac{\partial\tilde{\mathbf{E}}_p}{\partial r_1}\right)\cdot\left(\frac{\partial\hat{\mathbf{E}}_p}{\partial r_1}-\alpha(\hat{\mathbf{N}}\otimes\hat{\mathbf{N}})\frac{\partial\hat{\mathbf{E}}}{\partial r_1}\right)\mathrm{d}V_r \tag{30}$$

$$R_\varepsilon(\hat{\boldsymbol{\Xi}},\tilde{\boldsymbol{\Xi}}) = \int_{V_r}\left(\tilde{\varepsilon}+\beta v\frac{\partial\tilde{\varepsilon}}{\partial r_1}\right)\left(\frac{\partial\hat{\varepsilon}}{\partial r_1}+\sqrt{\frac{2}{3}}\left\|\frac{\partial\hat{\mathbf{E}}_p}{\partial r_1}\right\|\right)\mathrm{d}V_r \tag{31}$$

where $\tilde{\boldsymbol{\Xi}} = (\tilde{\mathbf{u}}, \tilde{\mathbf{E}}_p, \tilde{\varepsilon})$ is a suitable arbitrary weighting function and $\tilde{\mathbf{E}} = \frac{1}{2}(\nabla_{\mathbf{r}}\tilde{\mathbf{u}} + (\nabla_{\mathbf{r}}\tilde{\mathbf{u}})^T)$. Since eqn $(24)_4$ and $(24)_5$ are hyperbolic, the streamline upwind Petrov–Galerkin (SUPG) weighting functions (Brooks and Hughes, 1982; Johnson, 1987) are used in $R_{\mathbf{E}_p}$ and R_ε to stabilize the solution. Here β represents an artificial diffusivity acting only in the flow direction, the $\mathbf{v}$ (or $\hat{\mathbf{e}}_1$) direction, and its value is chosen to minimize the discrepancy between the finite element and the exact solutions (Brooks and Hughes, 1982).

Proper element choice is critical to the stability and accuracy of mixed methods. Since the plastic strain is incompressible, we use a quadrilateral element with nine nodes to interpolate the displacement $\mathbf{u}$ and four nodes to interpolate the plastic strain $\mathbf{E}_p$ and the cumulative plastic strain ε. Our element choice is motivated by the fact that a quadrilateral element that uses nine nodes for the velocity interpolation and four nodes for the pressure interpolation satisfies the Babuska–Brezzi criterion for Stokes' problem (Carey and Oden, 1983; Zienkiewicz and Taylor, 1991). Our element seems to behave satisfactorily as the numerical solution is free of spurious oscillations.

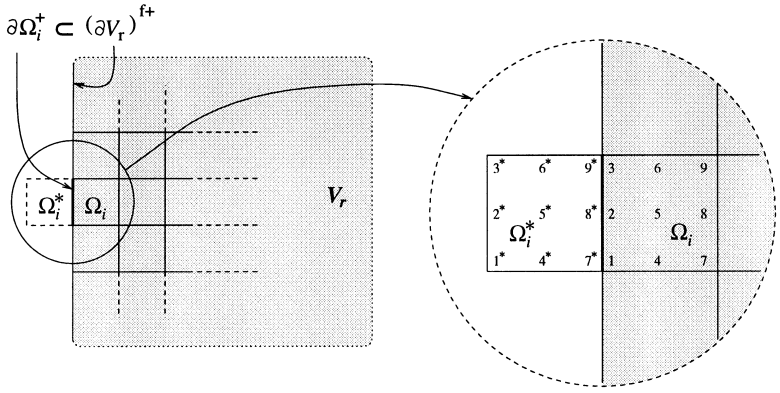

Fig. 4. Specification of boundary conditions across $(\partial V_r)^{f+}$.

For the thermal analysis we use a quadrilateral element with four nodes to interpolate the temperature field.

To accommodate the boundary conditions on the outlet boundary, we consider a typical element Ω_i on the outlet boundary (see Fig. 4). This element's contribution to the residual $R_{\mathbf{u}}$ is

$$R_{\mathbf{u}}^{\Omega_i} = \int_{\Omega_i} \tilde{\mathbf{E}} \cdot (\hat{\mathbf{C}}[\hat{\mathbf{E}} - \hat{\mathbf{E}}_p - \hat{\mathbf{E}}_t])\, \mathrm{d}V_r - \int_{\Omega_i} \tilde{\mathbf{u}} \cdot \hat{\mathbf{b}}\, \mathrm{d}V_r - \int_{\partial\Omega_i^+} \tilde{\mathbf{u}} \cdot \bar{\mathbf{t}}\, \mathrm{d}A_r \tag{32}$$

where $\partial\Omega^+$, is the element face on the outlet surface. However, $R_{\mathbf{u}}^{\Omega_i}$ cannot be computed directly since the value of $\bar{\mathbf{t}}$ is not known. The surface integral in the above residual represents the effect of the internal stress acting on the boundary of the control volume due to the material particles outside the control volume. This effect can be included by adding the internal force contributions from a fictitious neighboring element Ω_i^* (see Fig. 4) to element Ω_i i.e. by adding the internal nodal forces corresponding to nodes 7*, 8* and 9* in element Ω_i^* to those corresponding to nodes 1, 2 and 3 in element Ω_j. However, the nodal forces associated with element Ω_i^* are the same as the nodal forces associated with Ω_i since the fields are assumed to be well-developed and uniform in the r_1-direction. Hence the effect of the surface integral can be included by adding the internal nodal forces at nodes 7, 8 and 9 to nodes 1, 2 and 3, respectively, for every element Ω_i on the outlet boundary.

The weak formulation leads to a system of non-linear algebraic equations which are solved with the Newton–Raphson scheme. The tangential stiffness matrix is banded but not symmetric.

6. Numerical results

The RF formulation developed in the previous sections is used to analyze the steady state behavior of the laser surface treatment process shown in Fig. 8. An infinitely long plate is subjected to a laser load moving with velocity 0.005 m/s in the X_1 direction. The laser heat flux distribution is modeled as a Gaussian distribution. Convection heat transfer is imposed on both the top and

$$\mathbf{C} = 115.4\,\mathbf{II} + 153.8\,(\mathbf{I}\otimes\mathbf{I})\ GPa \qquad e = 486\ \theta\ kJ/K$$

$$f(\mathbf{S}_d, \epsilon) = \|\mathbf{S}_d\| - (700 + 30000\ \epsilon)\ MPa \qquad \rho = 7800\ kg/m^3$$

$$\mathbf{M} = 1 \times 10^{-5}\,\mathbf{I}\,K^{-1} \qquad \mathbf{K} = 51\,\mathbf{I}\,kW/m/K$$

$$q_{radiation} = \sigma\epsilon_r\,(\theta^4 - \theta_a^4) \qquad q_{laser} = \frac{P}{\pi r_b^2}\,Exp\left[\frac{2(r-r_0)^2}{r_b^2}\right] \qquad q_{convection} = h_c\,(\theta - \theta_a)$$

$$\sigma = 5.67 \times 10^{-8} W/m^2/K^4 \qquad P = 200W \qquad h_c = 50W/m^2/K$$

$$\epsilon_r = 0.8 \qquad r_b = 0.005m \qquad \theta_a = 298.15K$$

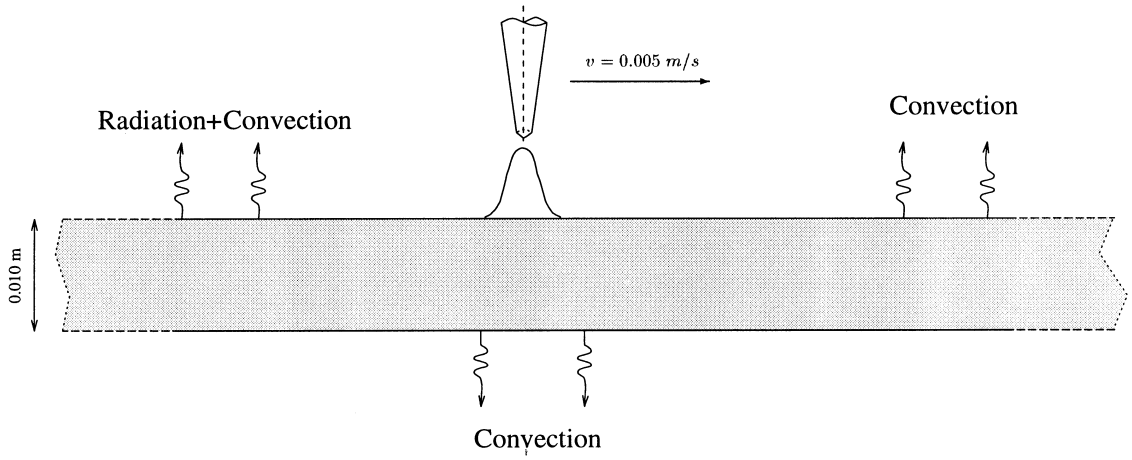

Fig. 5. Laser surface treatment: problem definition.

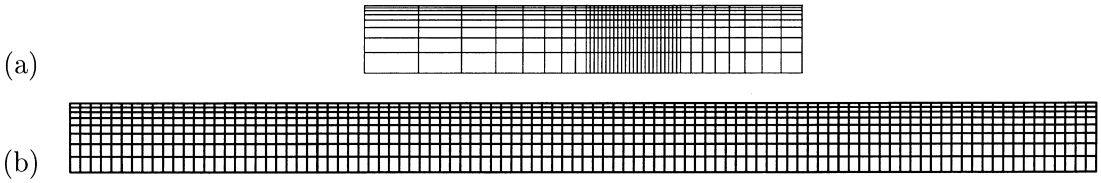

Fig. 6. The meshes for (a) RF analysis and (b) transient ABAQUS analysis.

bottom surfaces; radiation heat transfer is assumed to be significant only on that portion of the top surface which is exposed to the laser. The material and load data are provided in Fig. 5.

The domain for the RF analysis is 0.065 m long; the center of the laser is located 0.020 m from the inlet boundary. The discretization includes load mesh refinement in the region adjacent to the laser. A convergence study is performed (see the Appendix for details) and it is found that the 40×8 mesh shown in Fig. 6(a) is adequate. The thermal BVP is first solved and the resulting temperature field is used to generate the thermal loads in the mechanical BVP. The streamline

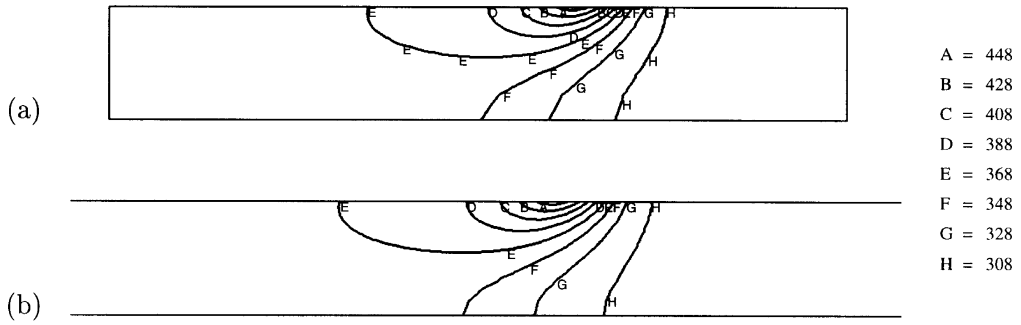

Fig. 7. Temperature plots from (a) RF analysis and (b) transient ABAQUS analysis.

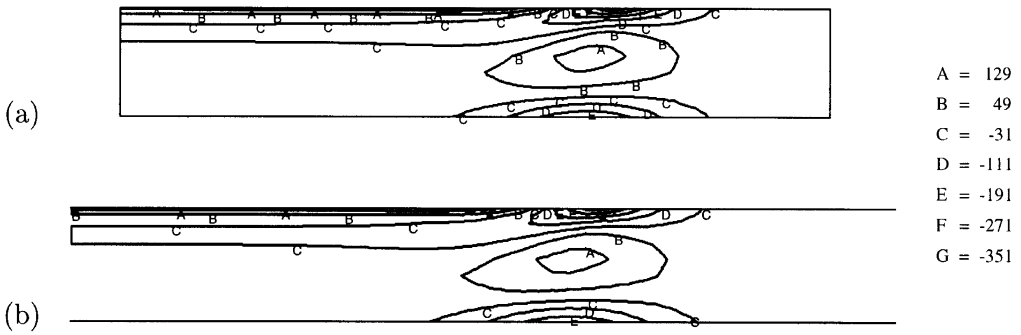

Fig. 8. S_{11} plots from (a) RF analysis and (b) transient ABAQUS analysis.

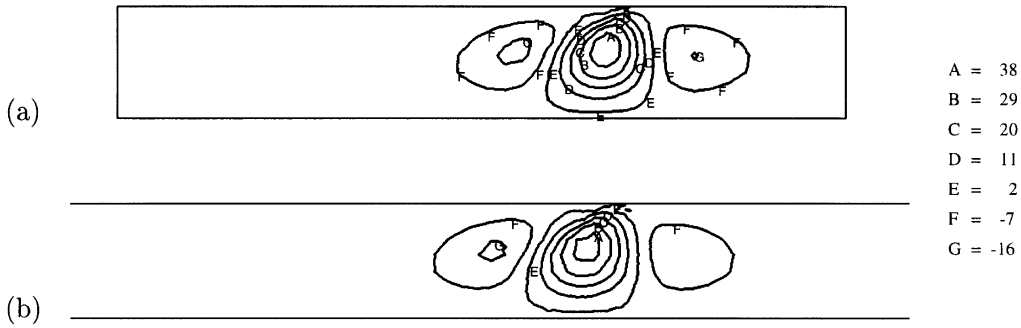

Fig. 9. S_{22} plots from (a) RF analysis and (b) transient ABAQUS analysis.

upwind Petrov–Galerkin weighing functions are used for the hyperbolic evolution equations, with a factor $\beta = 1.0$. Relaxation is used for the first few Newton iterations and then the standard Newton scheme is employed to obtain quadratic convergence. The temperature, stress, plastic strain and cumulative plastic strain contour plots appear in Figs 7–12.

For comparison purposes, the same problem is also analyzed via a transient Lagrangian analysis

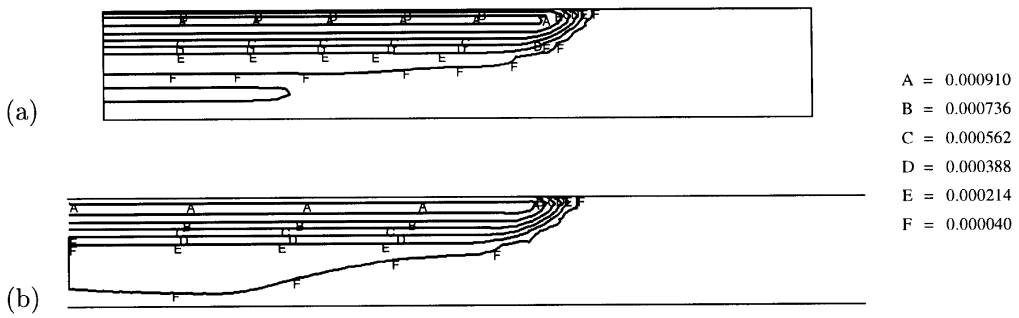

Fig. 10. E^p_{11} plots from (a) RF analysis and (b) transient ABAQUS analysis.

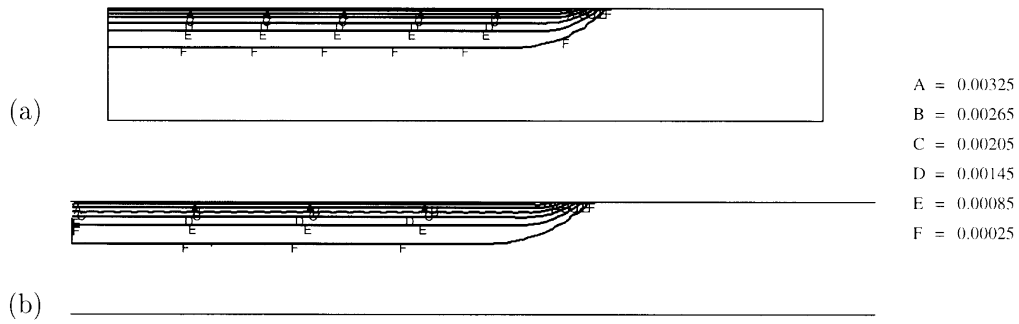

Fig. 11. E^p_{22} plots from (a) RF analysis and (b) transient ABAQUS analysis.

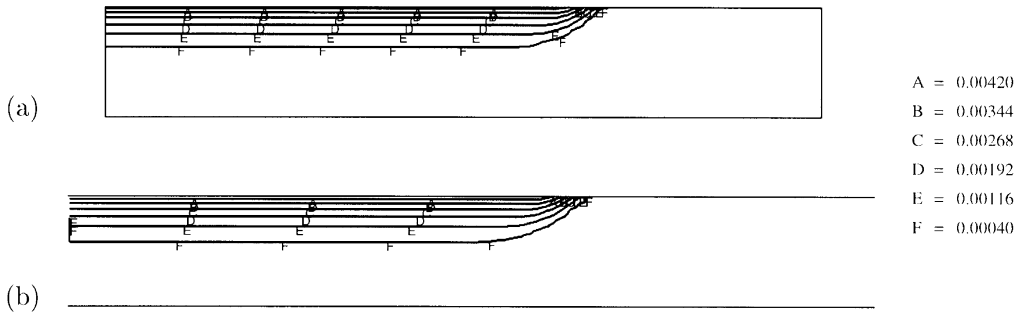

Fig. 12. ε plots from (a) RF analysis and (b) transient ABAQUS analysis.

Table 1
Results of mesh refinement study for the RF analysis

	16×80	16×40	16×20	8×80	8×40	8×20	6×80	6×40	6×20
$S_{11,\max}$	201	195	178	197	194	171	184	180	164
$S_{11,\min}$	−409	−408	−420	−408	−406	−418	−405	−402	−415
$S_{22,\max}$	44.1	44.5	44.5	43.5	44.3	43.9	44.6	44.2	44.7
$S_{22,\min}$	−18.0	−17.8	−17.7	−17.4	−18.3	−17.5	−18.4	−18.5	−18.7
$\text{Temperature}_{\max}$	459	458	459	459	458	459	459	458	458
$\text{Temperature}_{\min}$	299	299	298	298	299	299	299	299	299
$E^n_{11,\max}$ (10^{-4})	9.68	9.51	9.39	9.72	9.49	9.45	9.67	9.41	9.42
$E^p_{22,\max}$ (10^{-3})	3.81	3.77	3.44	3.79	3.79	3.41	3.73	3.76	3.41
$\varepsilon_{\max}$ (10^{-3})	4.80	4.79	4.05	4.78	4.78	3.98	4.69	4.70	4.02
CPU time (s)	1682.18	825.76	439.88	449.29	218.76	110.09	297.43	155.76	71.62
Memory (MB)	55.2	27.8	14.1	15.8	7.9	4.0	9.7	4.8	2.4

Table 2
Results of mesh refinement study for the Lagrangian analysis

	16×200	16×100	16×50	8×200	8×100	8×50	6×200	6×100	6×50
$S_{11,\max}$	187	187	187	184	184	182	160	160	157
$S_{11,\min}$	−393	−397	−382	−392	−394	−385	−386	−378	−385
$S_{22,\max}$	41.6	41.5	44.1	41.7	41.5	43.6	42.1	41.8	44.5
$S_{22,\min}$	−17	−17.4	−18.3	−17.4	−17.7	−18.3	−17.7	−17.9	−19.9
$\text{Temperature}_{\max}$	458	458	458	458	458	458	458	458	458
$\text{Temperature}_{\min}$	298	298	298	298	298	298	298	298	298
$E^p_{11,\max}$ (10^{-4})	9.81	9.78	9.79	9.72	9.68	9.82	9.95	9.99	9.83
$E^p_{22,\max}$ $(10^{-3)}$	3.74	3.76	3.83	3.73	3.75	3.81	3.59	3.62	3.69
$\varepsilon_{\max}$ (10^{-3})	4.81	4.83	4.91	4.80	4.83	4.90	4.70	4.74	4.80
CPU time (s)	8534.6	4159.4	2076.9	3968.8	1865.8	931.2	2785.9	1381.5	708.2
Memory (MB)	17.0	8.5	4.3	4.8	2.4	1.2	2.9	1.4	0.8

using ABAQUS. The domain for the Lagrangian analysis is a length 0.150 m. A convergence study is performed (also discussed in the Appendix) to consider the effects of the mesh size and the time step. The results converge for the 100×8 mesh shown in Fig. 6(b) and a time step of 0.1 s. Both analyses (thermal and mechanical) use eight noded elements; and reduced integration is used for the mechanical analysis to eliminate locking. The analogous results are shown in Figs 7–12, and are in good agreement with the results from the RF analysis.

The RF and Lagrangian analyses require 218.8 and 1865.8 CPU s, respectively, on the same IBM 590 machine, thus establishing the computational efficiency of the RF method. Another advantage of the RF formulation is the ability to locally refine the mesh at critical regions (see Fig. 6) thereby improving the spatial resolution of the response fields. However the unsymmetric

Table 3
Results of time increment refinement study for the Lagrangian analysis with the 8×100 mesh

Δt	0.05	0.1	0.2
$S_{11,\max}$	188	184	169
$S_{11,\min}$	−394	−394	−383
$S_{22,\max}$	41.6	41.5	38.8
$S_{22,\min}$	−17.7	−17.7	−16.8
$\text{Temperature}_{\max}$	458	458	458
$\text{Temperature}_{\min}$	298	298	298
$E^p_{11,\max}$ (10^{-4})	9.67	9.68	9.90
$E^p_{22,\max}$ (10^{-3})	3.77	3.75	3.67
$\varepsilon_{\max}$ (10^{-3})	4.84	4.83	4.81
CPU time (s)	3646.3	1865.8	1022.4

stiffness matrix and the increased number of degrees of freedom per element (due to the state variables), increases the memory requirement for the RF method. The RF analysis requires 7.9 MB of memory to store the stiffness matrix in unsymmetric, banded form vs 2.4 MB required to store the stiffness matrix in the symmetric banded form for the Lagrangian analysis.

7. Conclusions

A mixed Reference Frame formulation for quasi-steady thermo-elasto-plastic processes is developed for small deformation quasi steady processes that uses displacements and history-dependent variables as the primary variables. This formulation is then applied to simulate a laser-surface treatment process and the results agree with those obtained from a computationally intensive Lagrangian analysis.

Appendix : Mesh and time discretization studies

A convergence study is performed to analyze the effect of the mesh size on the RF results ; and the effect of the mesh size and the time step increment for the transient Lagrangian analysis. The maximum and minimum values of the axial stresses (S_{11} and S_{22}), temperature, and the maximum value of the plastic strains (E^p_{11}, E^p_{22} and ε) are monitored to determine when convergence is achieved. The results of the study are shown in Tables 1–3. It was concluded that the results converge to a sufficient degree with 8×40 mesh for the RF analysis ; and with a 8×100 mesh with a time step $\Delta t = 0.1$ s.

Acknowledgement

The research was supported by the National Science Foundation Grant NYI-DMI 9358132.

References

ABAQUS 5.6, 1996. Hibbitt, Karlsson and Soresen Inc., Providence, RI.

Agrawal, A., Dawson, P.R., 1985. A comparison of Galerkin and streamline techniques for integrating strains from an Eulerian flow field. International Journal of Numerical Methods in Engineering 21, 853–881.

Appleby, E.J., Lu, C.Y., Rao, R.S., Devenpeck, M.L., Wright, P.K., Richmond, O., 1984. Strip drawing : a theoretical–experimental comparison. International Journal of Mechanical Science 26 (5), 351–362.

Brooks, A., Hughes, T.J.R., 1982. Streamline upwind/Petrov–Galerkin formulations for convection dominated flows with particular emphasis on the incompressible Navier–Stokes equations. Computer Methods in Applied Mechanics and Engineering 32, 199–259.

Carey, G.F., Oden, J.T., 1983. Finite Elements—A Second Course. Prentice-Hall, New Jersey.

Carroll, J.T., Strenkowski, J.S., 1988. Finite element models of orthogonal cutting with applications to single point diamond turning. International Journal of Mechanical Science 30(2), 899–920.

CMAME, 1992. Reliability in computational mechanics. Computer Methods in Applied Mechanics and Engineering.

Dawson, P.R., 1978. Viscoplastic finite element analysis of steady-state forming processes including strain history and stress flux dependence. Applications of Numerical Methods to Forming Processes 28, 55–67.

Dawson, P.R., Thompson, E.G., 1978. Finite element analysis of steady-state elasto-visco-plastic flow by the initial stress-rate method. International Journal of Numerical Methods in Engineering 12, 47–57.

Ghosh, S., Kikuchi, N., 1991. An arbitrary Lagrangian–Eulerian finite element method for large deformation analysis of elastic-viscoplastic solids. Computer Methods in Applied Mechanics and Engineering 86, 127–188.

Ghosh, S. and Suresh, R., 1996. R-s adapted arbitrary Lagrangian–Eulerian finite element method for metal forming problems with strain localization. International Journal for Numerical Methods in Engineering 39, 3247–3272.

Haber, R.B., 1984. A mixed Eulerian–Lagrangian displacement model for large deformation analysis in solid mechanics. Computer Methods in Applied Mechanics and Engineering 43, 277–292.

Hu, Y.-K., Liu, W.K., 1993. An ale hydrodynamic lubrication finite element method with application to strip rolling. International Journal for Numerical Methods in Engineering 36, 855–880.

Huetink, J., Vreede, P.T., Lugt, J.V.D., 1990. Progress in mixed Eulerian–Lagrangian finite element simulation of forming processes. International Journal for Numerical Methods in Engineering 30, 1441–1457.

IJNME, 1991. Special issue on adaptive meshing. International Journal for Numerical Methods in Engineering.

Johnson, C., 1987. Numerical Solution of Partial Differential Equations by the Finite Element Method. Cambridge University Press, New York.

Lee, E.H., Mallet, R.L., Yang, W.H., 1976. Stress and deformation analysis of metal extrusion processes. Sudam Report, 76-2.

Lee, H.S., Haber, R.B., 1993. Eulerian–Lagrangian methods for crack growth in creeping materials. Advanced Computational Methods for Material Modeling—ASME 268, 141–153.

Liu, W.K., Belytschko, T., Chang, H., 1986. An arbitrary Lagrangian–Eulerian finite element method for path-dependent materials. Computer Methods in Applied Mechanics and Engineering 58, 227–245.

Liu, W.K., Chang, H., Chen, J.-S., Belytschko, T., 1988. Arbitrary Lagrangian Eulerian, Petrov–Galerkin finite elements for nonlinear continua. Computer Methods in Applied Mechanics and Engineering 68, 259–310.

Lubliner, J., 1990. Plasticity Theory, 1st ed. Macmillan, New York.

Ogden, R.W., 1984. Non-Linear Elastic Deformations. John Wiley and Sons, New York.

Palle, N., 1993. An adaptive mesh refinement scheme for solidification problems. Ph.D. thesis.

Rakotomalala, R., Joyot, P., 1993. Arbitrary Lagrangian–Eulerian thermomechanical finite-element model of material cutting. Communications in Numerical Methods in Engineering 9, 975–987.

Ruan, Y., 1996. Steady-state thermomechanical analysis of continuously quenched materials. Journal of Thermal Stresses 19, 395–416.

Strenkowski, J.S., Moon, K.-J., 1990. Finite element prediction of chip geometry and tool/workpiece temperature distributions in orthogonal metal cutting. Journal of Engineering for Industry 112, 313–318.

Thompson, E.G., Pittman, J.F.T., Zienkiewicz, O.C., 1983. Some integration techniques for the analysis of viscoelastic flows. International Journal for Numerical Methods in Fluids 3, 165–177.

Viriyauthakorn, M., Caswell, B., 1980. Finite element simulation of viscoelastic flow. Journal of the Non-Newtonian Fluid Mechanics 6, 245–267.

Zienkiewicz, O.C., Godbole, P.N., 1974. Flow of plastic and visco-plastic solids with special reference to extrusion and forming processes. International Journal of Numerical Methods in Engineering 8, 3–16.

Zienkiewicz, O.C., Taylor, R.L., 1991. The Finite Element Method, Vol. 2, 4th ed. McGraw-Hill.

Zienkiewicz, O.C., Jain, P.C., Onate, E., 1978. Flow of solids during forming and extrusion : some aspects of numerical solution. International Journal of Solids and Structures 14, 15–38.